scientific reports

Check for updates

OPEN

Characterizing Rock-Breaking Performance of PDC Cutters via Stability Metrics and Energy consumption in FDEM Simulations

Xinrui Wang[1,2], Hui Zhang[2]✉, Zhuoxin Dong[2,3,4], Jun Li[1,2], Cheng Qin[2,3,4], Boyuan Yang[2] & Yuting Zhou[2]

As oil production increasingly transitions from shallow to deep formation, the need for efficient PDC cutters to drill through deep hard rock becomes paramount. Currently, there is a lack of effective methods for optimizing cutter shapes and their cutting parameters. This study addresses this gap by developing a rock-breaking mechanism model for PDC cutters and proposing a Stability Index (SI) based on cutting force variations during the cutting process. Using the FDEM method, we simulated the rock-breaking processes of planar, stinger, and machete cutters under various cutting depths and angles. SI and Mechanical Specific Energy (MSE) were employed as evaluation metrics to analyze the rock-breaking characteristics and determine the optimal cutting parameters for each cutter type. The results indicate that at shallow cutting depths, cutting force changes are minimal, predominantly causing plastic damage to the rock, resulting in lower stress and reduced wear on the PDC cutters. Conversely, at greater cutting depths, significant fluctuations in cutting force occur, leading to brittle failure and the generation of large cuttings. This sudden increase in cutting force can accelerate rock breaking but also increases the risk of cutter wear. Our findings suggest that the planar cutter offers stable performance with high cutting force requirements, optimal at a cutting depth of 1.5 mm and an angle of less than 20°. The stinger cutter, requiring lower cutting forces, performs best at a cutting depth of 2 mm and an angle of 20°. The machete cutter exhibits characteristics similar to the stinger cutter at shallow depths and the planar cutter at deeper depths, making it suitable for drilling at a depth of 2 mm and an angle of less than 10°. By balancing SI and MSE, this study provides a comprehensive approach to optimizing PDC cutter performance, enhancing drilling efficiency while minimizing cutter wear.

From the last century to the present, fossil energy has played a very important role in the development of the world, meeting most of the world's energy needs[1–4]. As of 2019, the energy provided by oil and natural gas accounts for more than half of total energy production and is still the main energy supply method[5]. However, with the consumption of oil and natural gas, the exploitation of oil reservoirs gradually develops from shallow layers to deep layers. The high-strength rocks contained in deep strata, such as granite, basalt and quartzite, cause Polycrystalline Diamond Compact bits (PDC) to be affected by the drilling process. Therefore, how to efficiently destroy deep hard rocks has become the theme of oil field development[6,7].

The interaction between PDC bits and formation rocks is mainly related to drilling parameters, formation lithology, bit structure and surface morphology of PDC cutter. During the drilling process, the PDC cutter are in direct contact with the rock, and their surface morphology directly affects the rock breaking efficiency of the PDC, therefore, the selection of PDC cutter is very important for increasing the rate of penetration (ROP)[8,9].

In deep drilling, traditional planar cutter can no longer meet the needs of rapidly breaking high-hardness rocks, so more and more special-shaped cutters are designed to improve ROP. such as machete cutter, ax-shaped cutter, three-blade cutter and stinger cutter, etc. A large amount of research work has been carried out through indoor experiments and numerical simulations to evaluate the rock-breaking performance of these special-shaped cutters[10–12]. The machete cutter and stinger cutter have sharp shapes, which can fully damage rocks

[1]Petroleum College, China University of Petroleum at Karamay, Karamay 634000, China. [2]Petroleum Engineering College, China University of Petroleum (Beijing), 102249 Beijing, China. [3]National Engineering Laboratory for Exploration and Development of Low Permeability Oil and Gas Fields, Xi'an, China. [4]PetroChina Changqing Oilfield Company, Xi'an, China. ✉email: zhanghui3702@163.com

and are highly aggressive. They are suitable for cutting hard rocks[13–15]. The ax-shaped cutter's wear resistance and impact resistance have been significantly improved, which can extend the life of PDC drill bits. Its cutting performance is also slightly better than that of planar cutter (AX). Although the rock-breaking efficiency of the three-blade cutter is not as high as that of the machete cutter and stinger cutter with sharp cutting teeth, it consumes less energy for rock breaking[13]. Most of the above studies use traditional evaluation methods in the process of evaluating the rock breaking performance of PDC cutter, that is, cutting force and mechanical specific energy (MSE) are used as evaluation indicators. MSE represents the energy consumed in cutting unit volume of rock, which is simplified. The latter is the ratio of cutting force to cutting distance. These two evaluation methods are too simple and cannot distinguish the surface topography characteristics between different PDC cutters. In 2022, a rock-breaking efficiency evaluation index based on cutter sharpness was designed. By defining the PDC cutter surface morphology as the sharpness index and its ratio to MSE as the PDC evaluation criterion, both the PDC cutter surface morphology and the MSE were used as the evaluation criterion for PDC[16].

In summary, although the research on special-shaped PDC cutter has achieved certain results, there is still insufficient research on the evaluation method of PDC cutter's rock breaking efficiency. The traditional evaluation index cannot reflect the surface characteristics of the PDC cutter. Although the new evaluation method considers The influence of PDC cutters sharpness is eliminated, but the surface morphology characteristics of the cutters are simplified. Starting from the rock-breaking mechanism of PDC cutter, this article analyzes the different rock-breaking stages of PDC cutter and proposes a PDC cutter stability index (SI). Based on the index, a new method for evaluating the rock-breaking efficiency of cutting teeth and optimizing parameters is established.

Rock breaking mechanism and rock breaking performance evaluation index of PDC cutter

PDC cutter rock breaking mechanism model and cutting force response mode

Early studies on the rock failure modes during the rock breaking process of cutter can be summarized as plastic failure and brittle failure[17–20]. Its characteristic is that plastic failure mainly occurs when the cutting depth is shallow, when powdery cuttings are produced, and the cutting force fluctuates very little. Brittle failure occurs when the cutting depth is deep. At this time, large-volume block cuttings are produced, and the cutting force fluctuates greatly[21,22]. Meanwhile PDC will form a stress concentration area at the cutter tip during the rock breaking process. In this area, the rock failure is mainly plastic failure mode[23–26]. When the plastic zone is destroyed, the rocks around the plastic zone begin to crack and connect with each other, eventually causing the rocks around the zone to break into blocks and undergo ductile failure[27].

Figure 1 is a schematic diagram of the rock breaking mechanism of cutter Fig. 1(a) represents the plastic failure process when the cutting depth is shallow, Fig. 1(b) represents the brittle failure process when the cutting depth is deep. The cutting force comparison of the two failure regimes for sandstone is shown in Fig. 1[28]. In

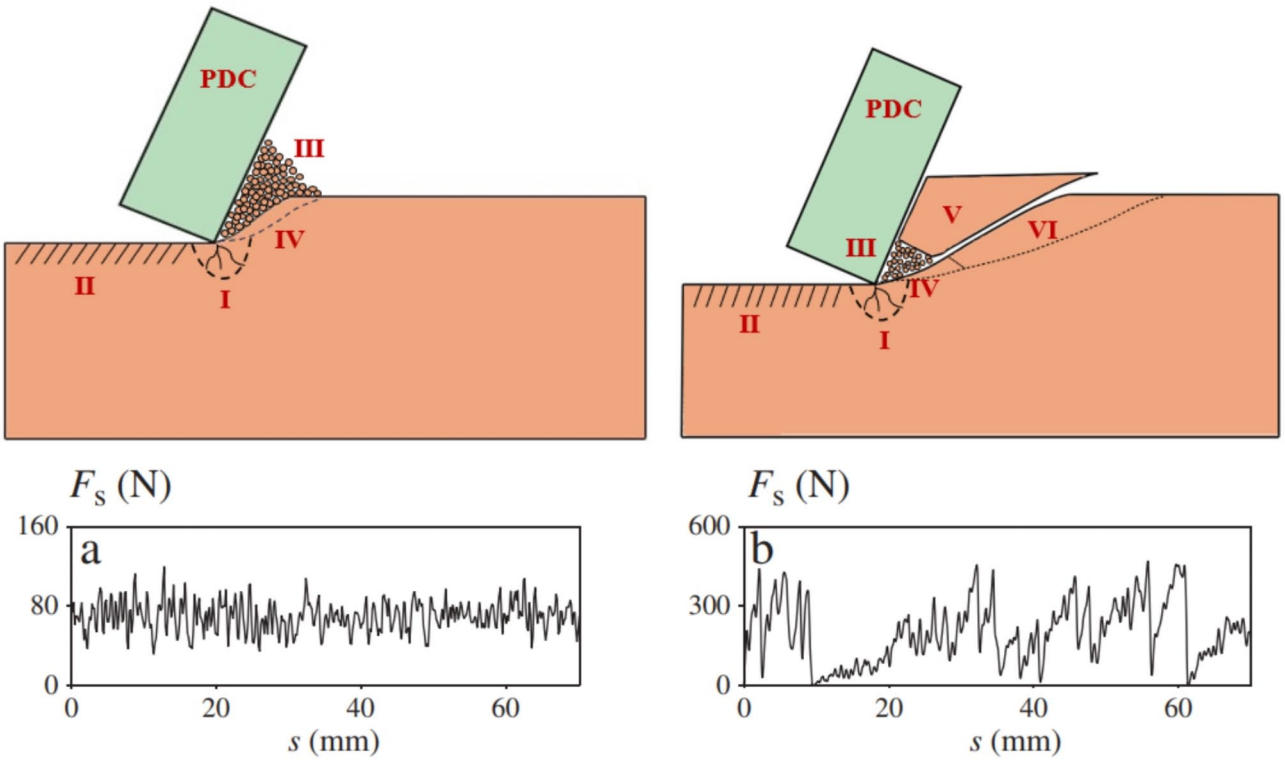

Fig. 1. Schematic diagram of PDC rock breaking mechanisms and shear forces[28].

general, the rock breaking process of PDC cutter starts from the crushing zone I at the tip of the cutters. In the vertical direction, it destroys the rock at the bottom of the PDC cutter, causing its strength to decrease and form the damage zone II. In the longitudinal direction, powdery cuttings are formed, and as the The extrusion of the cutter gradually discharges upward, forming the cuttings area III[15]. The cracks will spread from zone I to the surrounding rocks to form pre-crushed zone IV. As the PDC cutter continue to squeeze forward, zone IV will eventually be broken into rock cuttings and discharged. Compared with plastic damage, brittle damage has two more areas. Due to the limited influence range of crushing zone I, when the cutting depth is deeper, the rock cannot be completely destroyed. At this time, the PDC cutter will be in direct contact with the upper large rock, causing the damage crack in area III to expand upward, cutting off the rock in its entirety, and forming large cuttings V. After the area IV is completely destroyed, the cuttings VI will be peeled off in the form of cuttings V. This process is repeated. Complete the brittle failure process of rock[22].

During the brittle failure process, a large amount of energy (more than 90%) will be consumed in order to propagate cracks[29], which will lead to a surge in cutting forces. In order to better illustrate this process, sandstone with higher brittleness was selected as the object, as shown in Fig. 2. Figure 2.(a) shows the relationship between force and displacement when the cutting depth is shallow. It can be seen that the change of cutting force is relatively uniform, indicating complete plastic failure. Figure 2.(b) shows the relationship between force and displacement when the cutting depth is deep. It can be seen that the cutting force changes very drastically. According to the rock breaking mechanism, the curve can be divided into three types and they are related to the rock breaking mechanism. Correspondingly, the cutting force in section A of the curve is very small. The PDC cutter has just completed the brittle failure in the previous stage. The actual cutting depth at this time is very small, which corresponds to the transition from area III to area IV in Fig. 1. The cutting depth in section B of the curve increases, the cutting force increases, and the cutting force changes smoothly. The failure mode at this time is plastic failure, which corresponds to the crushing process in area IV. In section C of the curve, the cutting force surges, which is caused by the stripping of large rocks and the expansion of cracks, corresponding to area VI.

Evaluation index of PDC cutter during drilling process

The most commonly used method to evaluate the rock breaking efficiency of PDC cutter is to use mechanical specific energy (MSE), which was proposed by Teale in 1965[31]. This parameter represents the energy consumed in crushing unit rock.

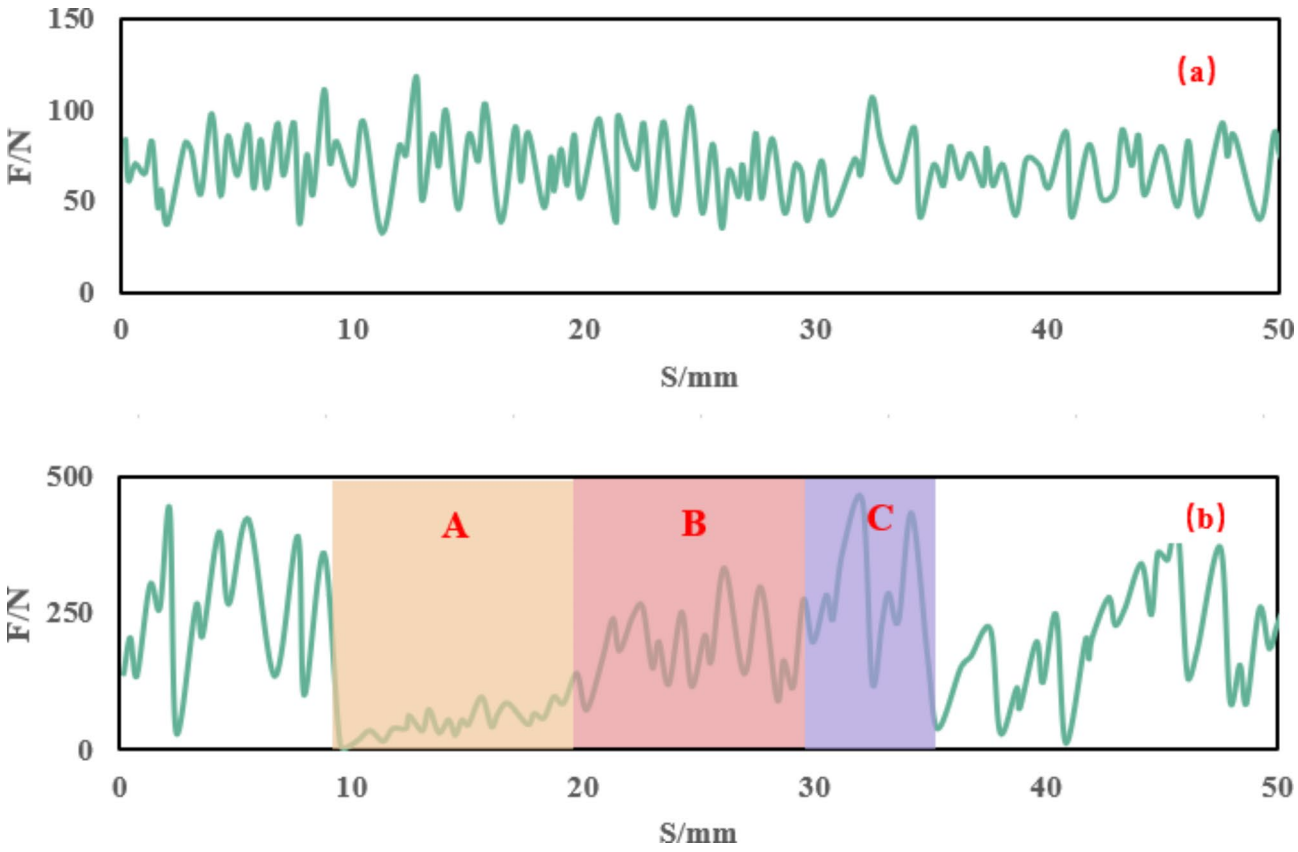

Fig. 2. (**a**) example of force signal (tangential component Fs) in the ductile mode (d = 0.6 mm)[28]; (**b**) example of force signal (tangential component Fs) in the brittle mode (d = 3 mm)[28,30].

$$MSE = \frac{W}{V} = \frac{\overline{F}_c}{A_c} \tag{1}$$

where *MSE* is mechanical specific energy (MPa); W is the total work consumed by rock crushing (J); V is the volume of rock crushing (mm^3); $\bar{F}_c$ is average cutting force (N); A_c is the projection of the cutter cutting into the formation on a vertical plane.

During the rock breaking process, it is generally hoped that the rock will have more volume of brittle failure. Brittle failure can produce large cuttings, thereby reducing the MSE and increasing the rock breaking efficiency[13]. The crushing zone around the cutter is very small, making it difficult to form through cracks[32,33]. This means that extremely high energy will be consumed during the brittle failure process, and large cutting force fluctuations will occur during this process, which will cause serious damage to the PDC cutter and reduce its subsequent rock breaking efficiency[34]. Therefore, for deep hard rock, the PDC cutter should maintain a stable cutting force as much as possible.

Figure 3 is a schematic diagram of the change curve of cutting force established based on the response relationship between cutting force and rock breaking mechanism. According to the PDC cutter rock breaking mechanism model, the change of cutting force can be divided into two stages, namely stable stage and fluctuation. stage. The failure mode of the rock in the stable stage corresponds to area III in Fig. 1 (a). At this time, the rock is plastically damaged, producing powdery cuttings, and the cutting force fluctuates little. The failure mode of rock in the fluctuation stage corresponds to area V in Fig. 1 (b). In order to form large cuttings, a large amount of energy is consumed, and the cutting force fluctuates greatly. The failure mode of this part of the rock is brittle failure. In hard rock, in order to make PDC more in the plastic failure mode, the energy consumed in the fluctuation stage should be reduced as much as possible. Therefore, the energy consumed in this stage accounts for a smaller proportion of the total energy consumed in the two stages, indicating that PDC The more stable it is. In order to quantify the stability performance of PDC, the PDC cutter stability index (SI) is proposed based on the interaction mechanism between PDC cutter and hard rock and the changing characteristics of cutting force:

$$SI = \frac{U_F}{U_{all}} \tag{2}$$

Where, SI is the PDC cutter stability index, dimensionless; U_F is the fluctuation energy of the fluctuation stage (relative to the energy consumed by the stage stage), J; U_{all} is The total energy consumed in the fluctuation stage and stable stage, J.

The calculation formula of U_F and U_{all} is

$$U_F = 0.5(F_{\max} - F_A)L_2 \tag{3}$$

$$U_{all} = F_{avg}(L_1 + L_2) + 0.5(F_{\max} - F_A)L_2 \tag{4}$$

Where, L_1 is the stable stage displacement. mm; L_2 is the fluctuation stage displacement. mm; F_{max} is the maximum force of the cutting force curve of s fluctuation. stage, N; F_{max} is the average cutting force of the fluctuation stage and the stable stage, N; F_a is the average cutting force of the stable stage, N.

If SI is calculated according to this expression, the parameters that require statistics are too cumbersome, so it is simplified based on the expression of the average cutting force F_{avg}.

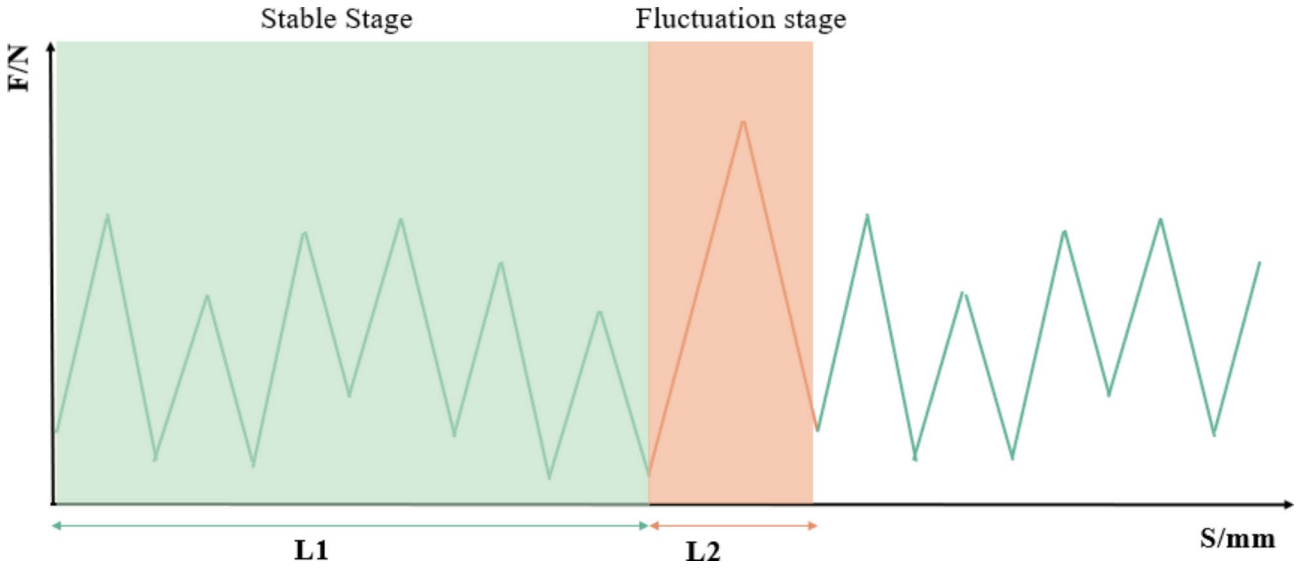

Fig. 3. Schematic diagram of PDC cutter rock breaking cutting force changing with cutting distance.

$$F_{avg} = \frac{F_a L_1 + 0.5\,(F_{\max} + F_a)\,L_2}{L_1 + L_2} \tag{5}$$

The ratio of L_1 and L_2 can be derived:

$$\frac{L_2}{L_1} = \frac{F_{avg} - F_a}{0.5\,(F_{\max} + F_a) - F_{avg}} \tag{6}$$

Substitute formula 3, formula 4 into formula 2:

$$SI = \frac{0.5\,(F_{\max} - F_a)\,\frac{L_2}{L_1}}{F_a + 0.5\,(F_{\max} - F_a)\,\frac{L_2}{L_1}} \tag{7}$$

Bring formula 6 into formula 7 to simplify the formula:

$$SI = 1 - \frac{F_a}{F_{avg}} \tag{8}$$

SI describes the proportion of energy consumed in the fluctuation. stage for cutting large volumes of rock to the energy consumed in the stable stage and fluctuation stage. When there is no fluctuation stage, it represents pure plastic failure of the rock, at that time the value of SI is 0. With the proportion of plastic damage decreases, SI gradually increases and finally reaching a maximum of 1, at that time the failure mode of the rock is brittle failure.

PDC cutter rock breaking model based on FDEM

Principle of the coupling finite element and cohesive element

In the traditional finite element simulation, the failure behavior of rock is often described by deleting the elements whose deformation reaches the upper limit. In the rock-breaking simulation, the deformation of the element in direct contact with the cutter is the largest, so the destruction of the rock is carried out close to the cutter. However, in the actual process of rock breaking, cracks will gradually form near the area where the cutter contacts the rock, and these cracks will expand and connect with each other to gradually form a broken area. Therefore, rock breaking occurs in a small area near the cutter. The traditional finite element simulation cannot describe this crushing phenomenon very well. Even if a small area of the unit is deleted at the same time, it will lead to a calculation error that the force of the tool is zero after the element is deleted due to the lack of contact objects. By introducing cohesive elements, the combination of cohesive elements and finite elements can well make up for the shortcoming.

As shown in Fig. 4(a), a cohesive element without thickness is inserted between two finite element to form the complex in Fig. 4(b) (the block in the figure is only for demonstration and does not represent the final element shape), in order to after inserting the cohesive element, a continuous model is obtained. The upper and lower surfaces of the cohesive element should share nodes with the finite elements on both sides respectively to ensure the continuity of the model, as shown in Fig. 4(c). before the rock cracked. The force of the area is calculated by the finite element and transmitted to the cohesive element As the force increases, the cohesive element is

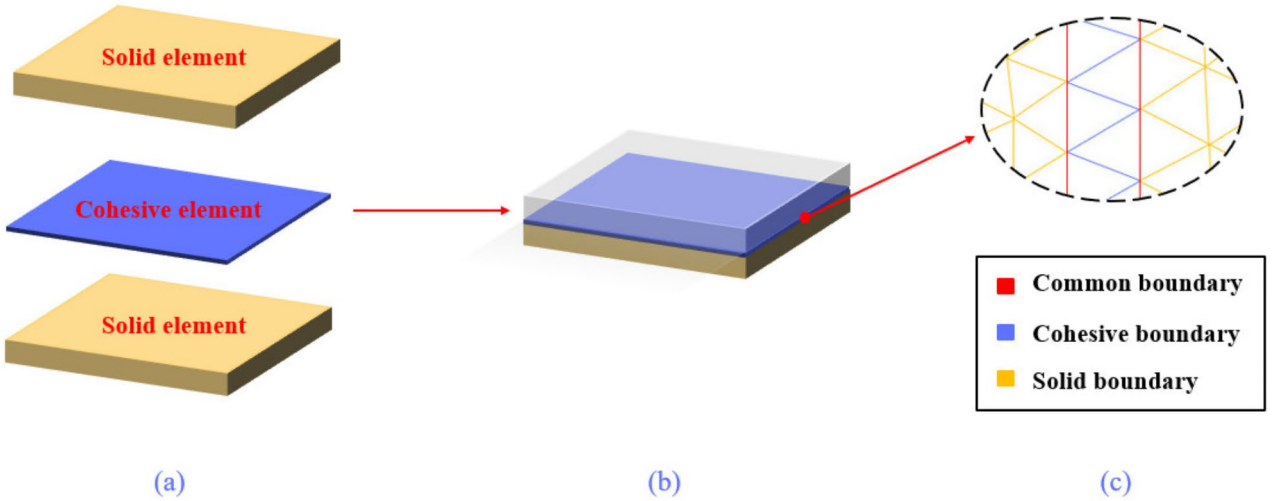

Fig. 4. The insertion process of cohesive elements and the distribution of nodes between the two elements.

destroyed. When all the cohesive elements near a finite element are destroyed, the finite element falls off from the model, representing At this time, the cohesive element without thickness is destroyed, and the finite element itself will not be destroyed. With the movement of the cutter, the detached finite element will be gradually compressed or excluded, and the force will be transmitted during this process.

As shown in Fig. 5, the cohesive element has two failure modes, one is tension and the other is shear. The two failure modes of the cohesive element are distinguished in a similar way, that is, they all follow the traction separation criterion, that is, through the relative displacement is used to judge the connection between two finite elements. The destruction of the cohesive element will go through three stages. The first stage is the elastic stage. At this time, the stress increases linearly with the displacement, and the element has not yet been damaged. The

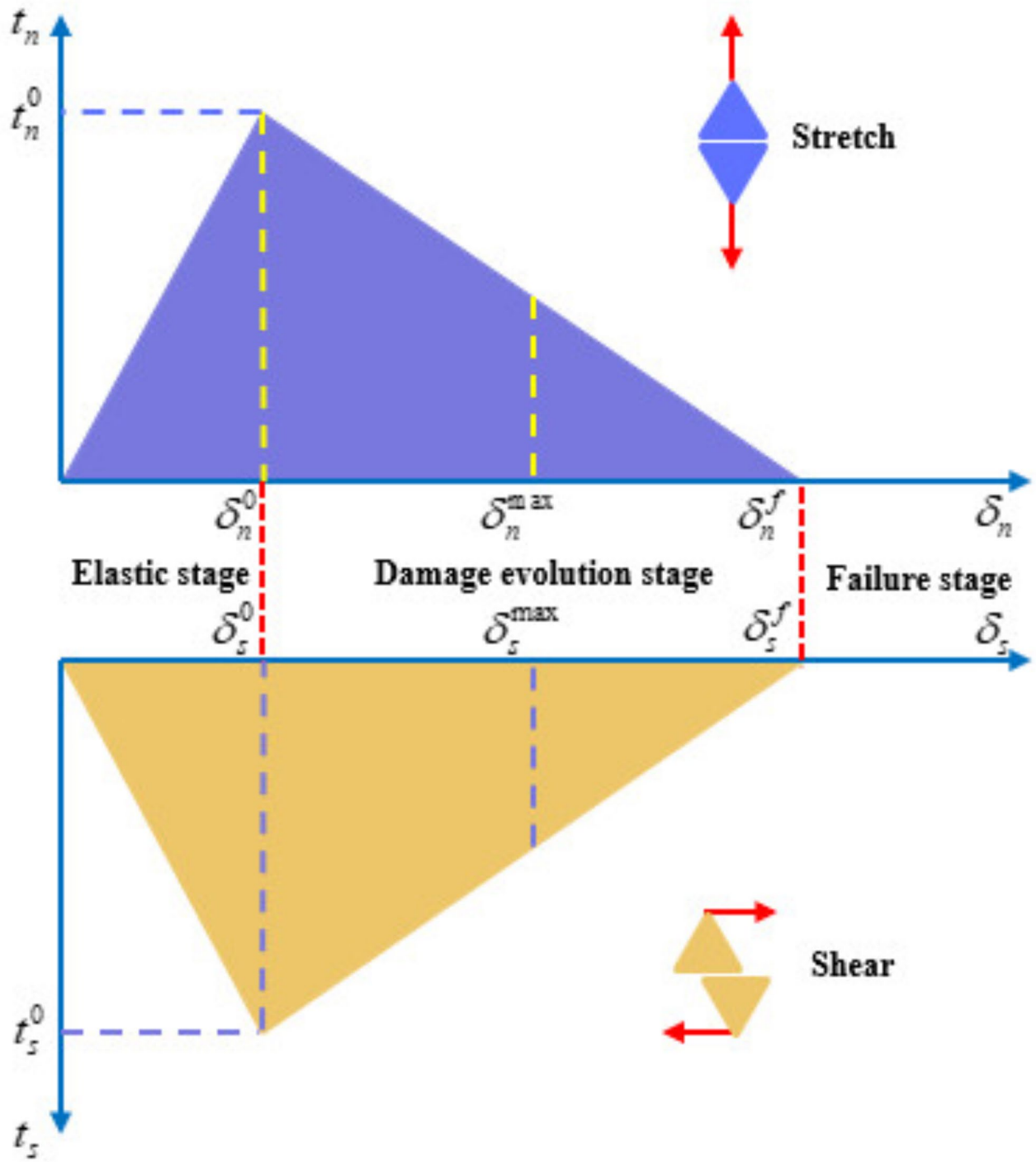

Fig. 5. The insertion process of cohesive elements and the distribution of nodes between the cohesive element and finite element.

Properties	Unit	Values
Young's Modulus	GPa	46
Poisson's Ratio		0.2
Density	g/cm^3	2.46
Stiffness (Normal)	N/mm	9000
Stiffness (First, Second)	N/mm	6000
Norminal Stress (Normal)	MPa	60
Norminal Stress (First, Second)	MPa	80
Fracture Energy (Normal)	N/mm^2	0.03
Fracture Energy (First, Second)	N/mm^2	0.04

Table 1. Numerical simulation of rock mechanics parameters.

second stage is the damage evolution stage. When the displacement is greater than the initial displacement of the damage ($\boldsymbol{\delta^0}$), The cohesive element begins to accumulate damage, and the third stage is the failure stage ($\boldsymbol{\delta^f}$). When the displacement exceeds the complete failure displacement, the cohesive element is destroyed. The stress changes in tension and shear are shown in Eqs. 9 and 10, respectively:

$$t_n = \begin{cases} k_n\delta_n & \delta_n \leqslant \delta_n^0 \\ (1-D_n)\, k_n\delta_n & \delta_n^0 \leqslant \delta_n \leqslant \delta_n^f \\ 0 & \delta_n^f \leqslant \delta_n \end{cases} \tag{9}$$

Where t_n is the tensile stress, k_n is the material stiffness in the tensile direction, δ_n is the displacement in the tensile direction, and D_n is the damage variable in the tensile direction. $\delta_n^{\,0}$ is the initial damage value in the tensile direction, and $\delta_n^{\,f}$ is the complete damage displacement in the tensile direction.

$$t_s = \begin{cases} k_s\delta_s & \delta_s \leqslant \delta_s^0 \\ (1-D_s)\, k_s\delta_s & \delta_s^0 \leqslant \delta_s \leqslant \delta_s^f \\ 0 & \delta_s^f \leqslant \delta_s \end{cases} \tag{10}$$

Where t_s is the shear stress, k_s is the material stiffness in the shear direction, δ_s is the displacement in the shear direction, and D_s is the damage variable in the shear direction. $\delta_s^{\,0}$ is the initial damage value in the shear direction, and $\delta_s^{\,f}$ is the complete damage displacement in the shear direction.

$$D = \frac{\delta^f\left(\delta^{\max} - \delta^0\right)}{\delta^{\max}\left(\delta^f - \delta^0\right)} \tag{11}$$

Where δ^0 is the displacement when the cohesive element starts to damage, δ^f is the displacement when the cohesive element is completely destroy, δ^{max} is the maximum displacement of the cohesive element during the loading process, and D is the damage factor. When $D=0$, it means that the cohesive element has no damage and is in the elastic stage. When $0<D<1$, it means that the cohesive element begins to suffer damage and is located in the damage evolution stage. When $D=1$, it means that the cohesive element has been damaged and is in the failure stage.

The model uses the maximum nominal stress criterion to define the failure behavior of the cohesive element, that is, when the displacement in any direction reaches the maximum marked stress in this direction, the element begins to damage

$$\max\left\{\frac{t_n}{t_n^0}, \frac{t_s}{t_s^0}, \frac{t_t}{t_t^0}\right\} = 1 \tag{12}$$

Where t_n and t_s are the stresses in the tensile and shear directions respectively, and $t_n^{\,0}$ and $t_s^{\,0}$ are the nominal stresses in the tensile and shear directions respectively, t_t and $t_t^{\,0}$ are the shear stress values in the direction of the other side.

Stress and strain can be converted according to formula 5:

$$\begin{bmatrix} t_n \\ t_s \\ t_t \end{bmatrix} = \begin{bmatrix} E_{nn} & & \\ & E_{ss} & \\ & & E_{tt} \end{bmatrix} \left[\frac{\delta_n}{T_0}, \frac{\delta_s}{T_0}, \frac{\delta_t}{T_0}\right]^{\mathrm{T}} \tag{13}$$

Where E is the material stiffness in the tensile direction and the two shear directions, and T_0 is the initial thickness of the cohesive element, which is set to 1 to eliminate the singularity of the stress.

Rock mechanical properties

Before carrying out numerical simulation, it is necessary to set the micromechanical parameters of rock materials. Generally, the rock model has the mechanical properties of real rocks through trial and error method. The microscopic parameters are continuously adjusted to make the uniaxial compression and uniaxial tension numerical simulation experimental results consistent with Real uniaxial compression and uniaxial tensile experimental results are compared. This article also adopts this method for comparison. At the same time, the research object of this article is hard rock. On the premise of reaching the rock strength, it only needs to comply with the mechanical characteristics of the rock material. Therefore, it is not compared with the indoor macro mechanical performance test. The pressure resistance The numerical simulation model of the experiment and tensile experiment was based on the model used by Hongxiang Jiang[35]. The calibrated micromechanical parameters are shown in Table 1.

As shown in Fig. 6, it is the stress-strain curve of the compressive test and tensile test of the rock during the calibration process. Figure 6 (a) is the simulation result of the digital simulation experiment of the compressive test, and its compressive strength reached 117.3 MPa. Figure 6 (b) is the simulation result of the tensile test digital simulation experiment, and the tensile strength reaches 16.8 MPa. Some fluctuations can be observed, this phenomenon is attributed to the localized stress concentration caused by the indenter contacting the rock at a certain velocity. Two numerical simulation test experiments have proven that the micromechanical parameters in Table 1 are consistent with the changing characteristics of hard rock, it is ensured that the rock strength meets the hard rock condition for subsequent research.

Simulation of PDC cutting experiment model

In order to make the experimental results of numerical simulation more accurate, the grid needs to be partially refined. Through the adaptability analysis of the grid size, when the unit size is between 1 mm and 0.2 mm, there is not much difference in the numerical calculation results, but the smaller the unit size, the better the rock breaking effect. If small units are used for global calculations, the calculation cycle will often be too long due to the large amount of calculations. Therefore, in order to take into account both computational efficiency and simulation effect, the model is divided into two parts according to the unit size. The first part is the encrypted area with a unit size of 0.5 mm. This part is the area where the PDC tool interacts with the rock. This area is a cuboid with a length, width, and height of 15, 12, and 6 mm respectively. This is the area between the cutter and the rock. Areas of model interaction. The second part is the stress transfer area, which is responsible for conducting stress. The unit size is 1 mm. The main function of this part of the area is to transfer stress to the boundary. The length, width, and height of the model are 30, 30, and 15 mm respectively. The mesh type is selected as tet mesh, and the cutter move in the Y direction at a fixed speed of 5 mm/s to directly break the rock. The established PDC cutting model and PDC cutters are shown in Fig. 7.

Model validation

In this section, we validate the previously established model using a planar cutter as an example. As shown in Fig. 8(a), during the process of breaking hard sandstone at a cutting depth of 2 mm, a small fracture pit measuring 3 mm in length forms due to the initiation and propagation of cracks ahead of the cutter. This results in the detachment of flaky rock cuttings, which can be observed around the cutter. The numerical simulation results, depicted in Fig. 8(b), show areas of plastic deformation in the rock mesh. Similar to the experimental observations, cracks initiate and propagate in front of the cutter, leading to rock failure and the formation of approximately 3 mm rock fragments. As the cutter advances, these fragments are detached, forming small fracture pits consistent with the experimental phenomena.

Figure 9(a) illustrates that as the cutter moves forward with the same cutting depth, larger rock fragments and fracture pits are produced. This indicates that at a cutting depth of 2 mm, the fracturing characteristics of the igneous rock remain brittle, and the size of the rock cuttings varies. To enhance readability, some rock cuttings

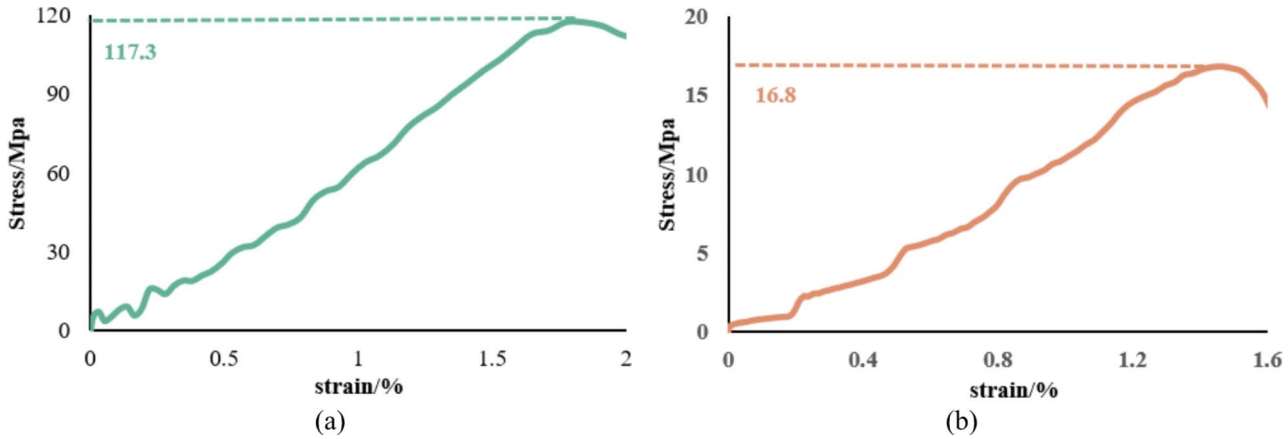

Fig. 6. (**a**) Numerical simulation stress-strain curve of compression test (**b**) Numerical simulation stress-strain curve of tensile test.

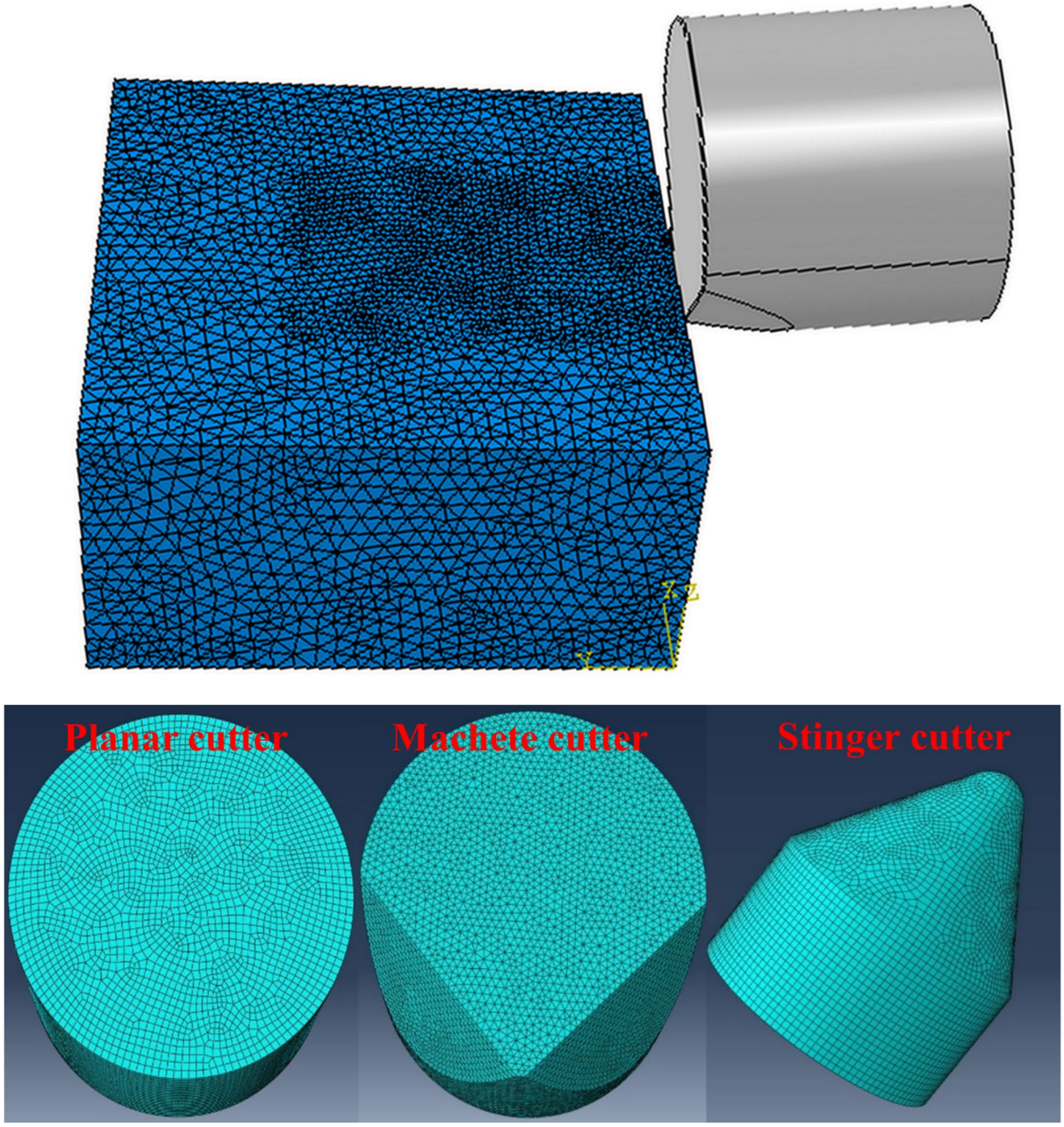

Fig. 7. Numerical simulation model of PDC cutter cutting rock and three cutter shapes used.

in front of the cutter was manually removed to better observe the model's damage, as shown in Fig. 9(b). The numerical simulation also shows crack initiation on both sides of the cutter, extending forward and towards the center of the cutter, resulting in larger fragments that are subsequently detached, forming fracture pits similar to those in the experiments. Single rock mesh elements are expelled, and the experimental images reveal that not only large fragments but also powdery and small particulate cuttings are present during the fracturing process, further demonstrating the model's accuracy.

In summary, the breaking morphology and characteristics simulated by the established model are highly consistent with experimental observations, validating the model's accuracy. This model can thus be utilized for further studies.

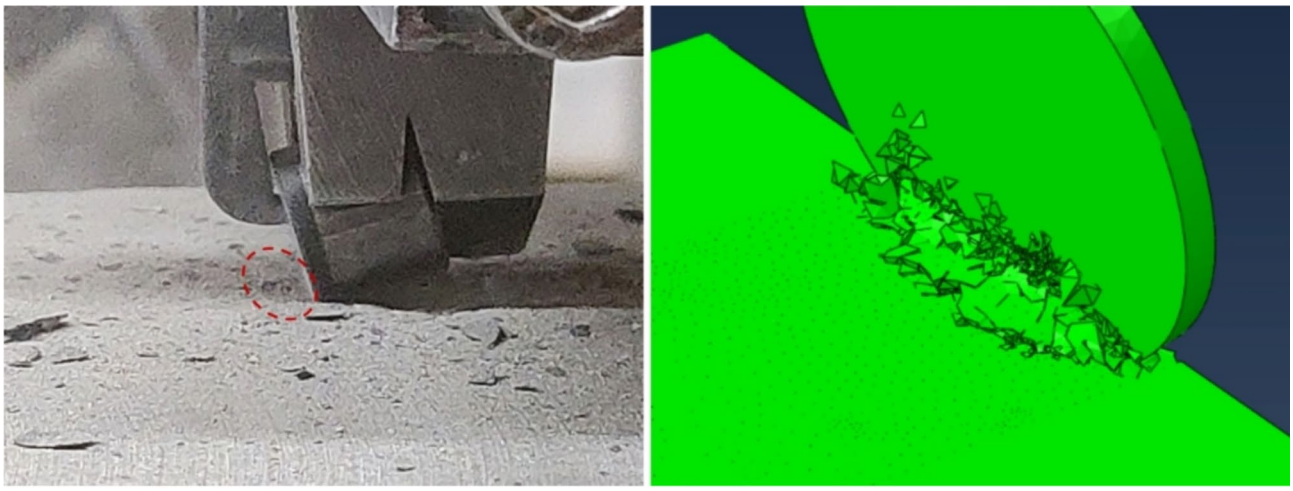

Fig. 8. (**a**) Experimental diagram of the formation of a small crushing pit by planar cutter breaking hard sandstone, (**b**) numerical simulation diagram of the small crushing pit.

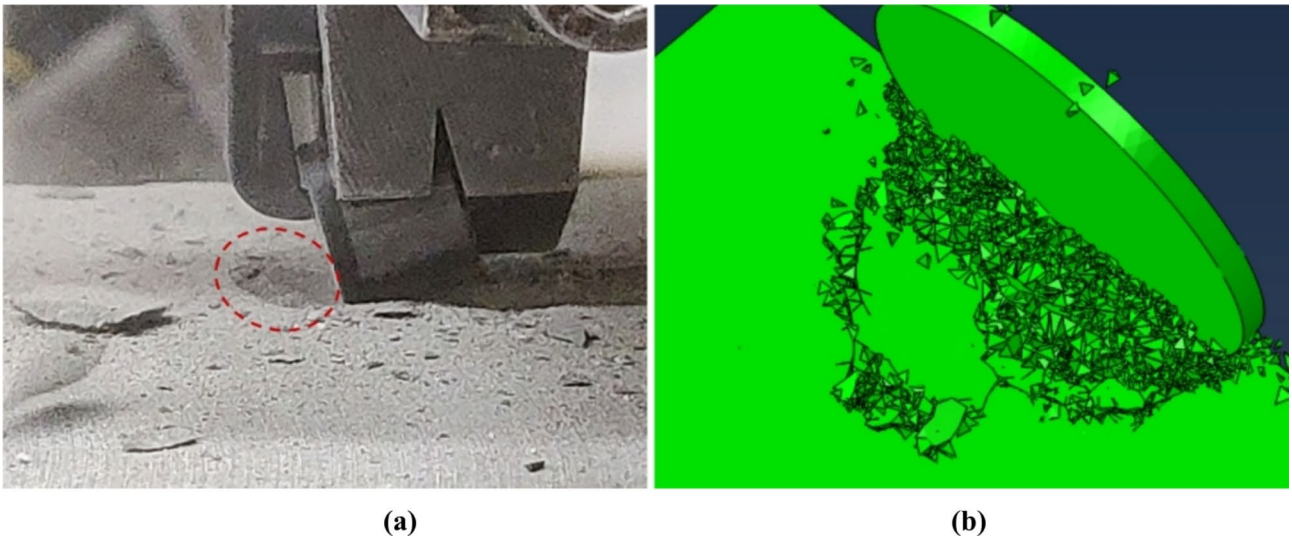

Fig. 9. (**a**) Experimental diagram of the formation of a large crushing pit by planar cutter breaking hard sandstone, (**b**) numerical simulation diagram of the large crushing pit.

Results and discussion

Analysis of rock breaking process and characteristics of PDC cutters

This article mainly analyzes the stability of the cutter, not the differences between the shaped cutters. The cutting force fluctuation of plastic failure is relatively stable, and the stability problem is not prominent. At the same time, simulations found that all three types of cutters can breaking rocks in the regime of brittle failure. Therefore, this chapter mainly compares the stability of the three types of cutter in brittle regime.

As shown in Fig. 10(a), when the cutting angle is 20°, as the cutting depth increases, the overall lengths of stages I and II extend to varying degrees. This is because the increase in cutting depth causes The rock-breaking stage increases, and the cutter need to break more rocks and thus form a larger crushing stage. As the crushing stage of the PDC cutter becomes larger, the PDC cutter in stage III can move stably for a longer distance. Therefore, the increase in the depth of the cutter will cause the rock-breaking period of the PDC cutter to become longer. When the cutting depth changes from 0.5 mm to 2.5 mm, the rock-breaking period of the planar cutter gradually increases from 0.674 mm to 1.1 mm.

As shown in Fig. 10(b), when the cutting depth is 2 mm, as the cutting angle changes, the change in stage I is not obvious. This is because the rock-breaking stage of the cutter does not change much between different cutting angles. There is a significant extension in stage II, indicating that the increase in cutting angle will lead to an enlargement of the crushing stage of the PDC cutter. However, the stage II has become shorter, which shows

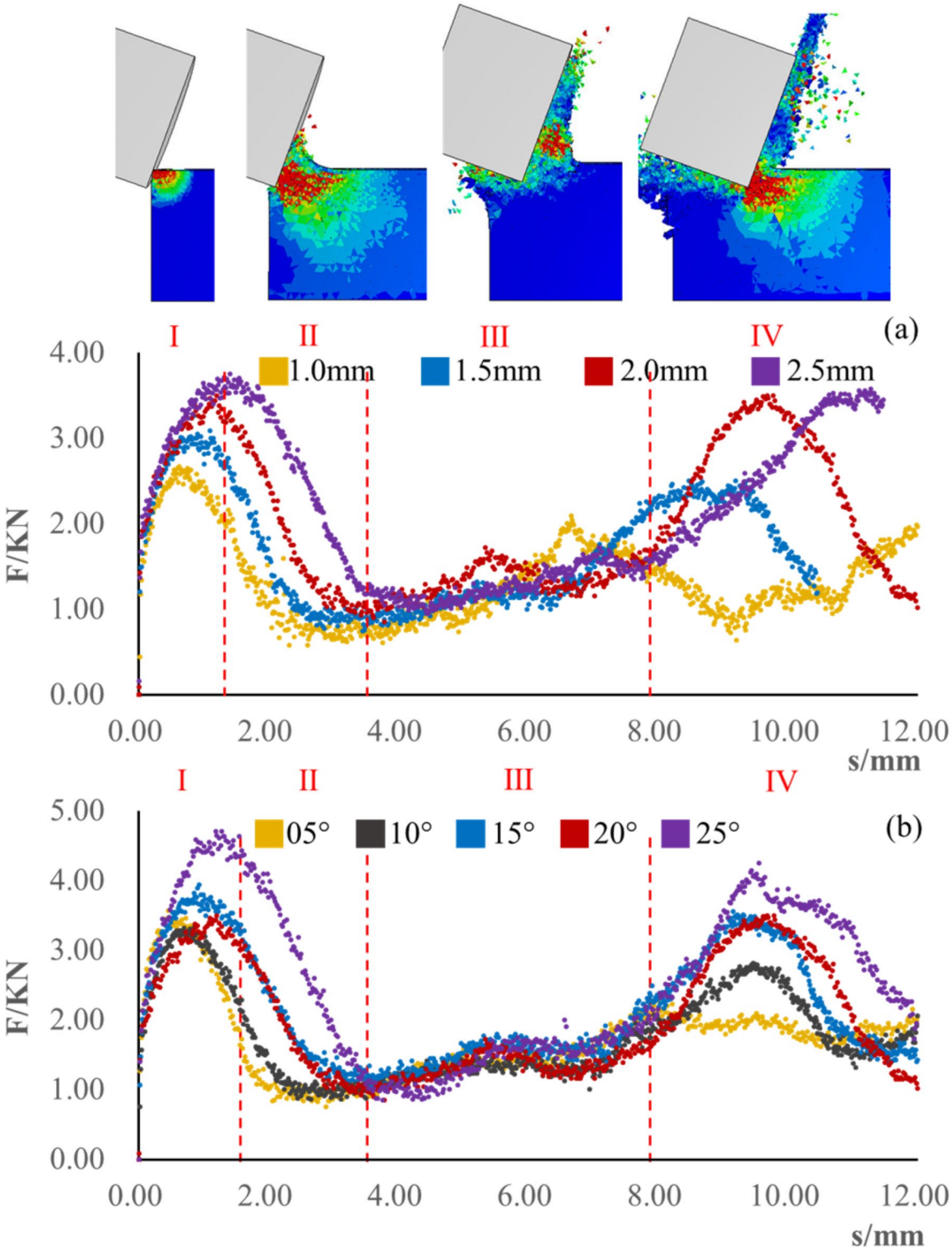

Fig. 10. The rock-breaking process and cutting force change curve of planar cutter.

that although the crushing stage in the second stage has become larger, the stress has become more concentrated, and only part of the rock in the crushing stage can be broken, resulting in a shorter PDC cutter stable stage. The cutting angle only affects rock breaking stage, but has little effect on the overall rock breaking cycle.

As shown in Fig. 11, it is the cutting force change curve of the stinger cutter. It can be seen from the curve changes that the main cutting processes of the stinger cutter are stages I, II and IV. The length of stage III is very short, It shows that the stinger cutter removes cuttings very quickly, another reason is that the range of broken rocks by the stinger cutter is smaller than that of the planar cutter. As shown in Fig. 11(a), the stinger cutter is

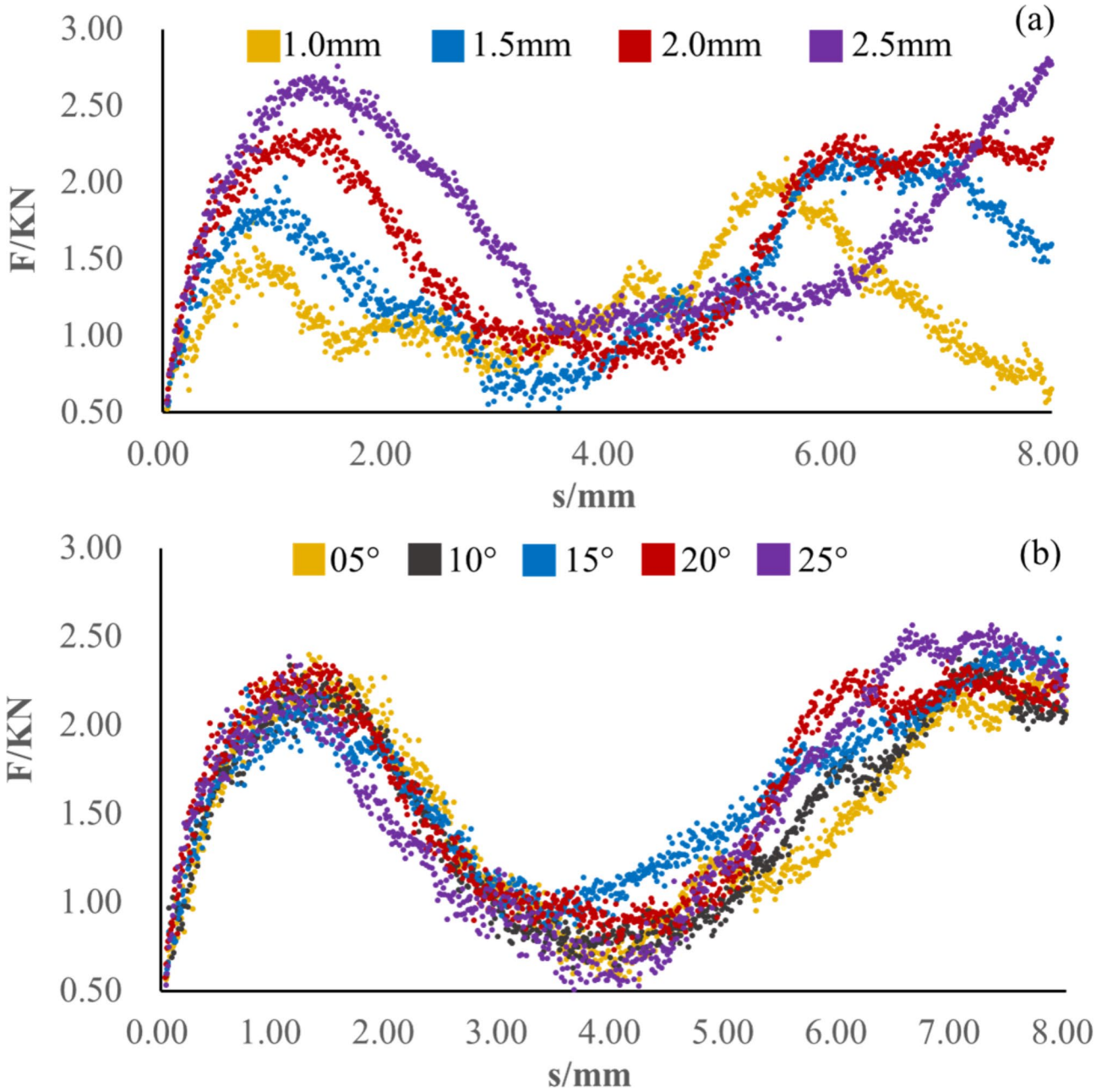

Fig. 11. Cutting force change curve of stinger cutter.

highly sensitive to the cutting depth. As the cutting depth increases, more and more cutting forces are required to increase the cutting depth of the same magnitude. This is due to the stinger cutter is relatively sharp and the cutting stage changes drastically. But in general, the stinger cutter requires less cutting force and is more suitable for breaking rocks at more cutting depths than the planar cutter. As shown in Fig. 11 (b), the stinger cutter is not highly sensitive to the cutting angle and the cutting force does not change greatly during the change of the cutting angle. As the cutting angle increases, the cutting force in stages I and II decreases slightly. This is because the cutting angle slightly reduces the cutting stage, resulting in a decrease in cutting force. The cutting forces in stages III and IV increase slightly. This is Because the increase of the cutting angle causes the cutter tip stress to spread to farther rocks during the cutting process, the actual broken rock volume becomes larger.

As shown in Fig. 12, it is the cutting force change curve of the machete cutter. The cutting process is similar to the characteristics of planar cutter. As shown in Fig. 12(a), as the cutting depth increases, the lengths of Stage I, Stage II and Stage III all increase significantly, resulting in a rapid rock-breaking period. This is because as the cutting depth increases, The rock-breaking stage of the machete cutter increases more quickly than the planar cutter, resulting in a significant change in the range of the crushing stage at the cutter tip. machete cutter. When the cutting depth is shallow, the cutting force required by the machete cutter to break the rock is very small and the range of region III is very short. At this time, the cutting force change is similar to the stinger

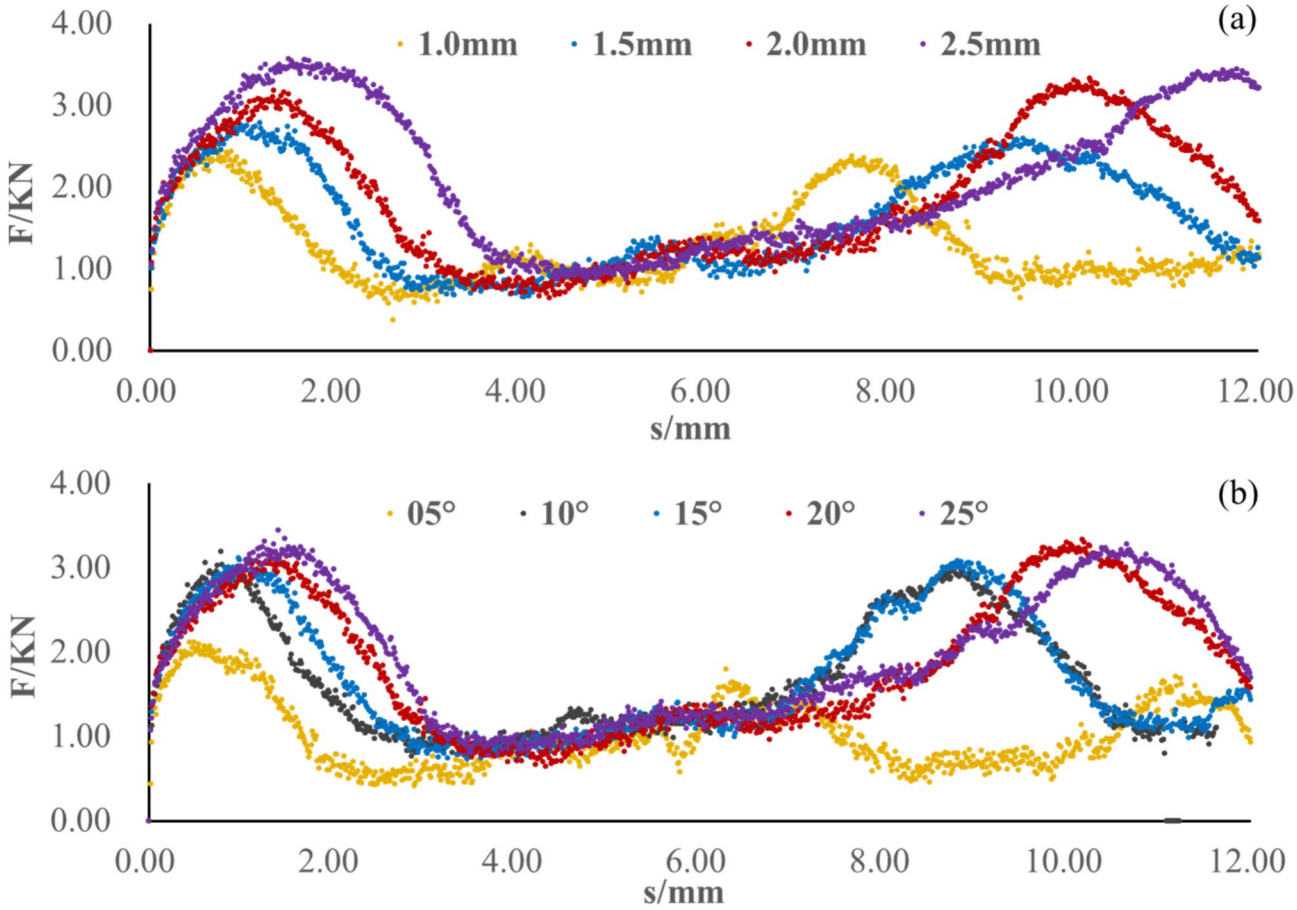

Fig. 12. Cutting force change curve of machete cutter.

cutter, indicating that the machete cutter can break the rock during the cutting process. Easier to insert into the ground. When the cutting depth is deeper, the cutting force change curve of the machete cutter has some of the changing characteristics of the planar cutter. At this time, the cutting force curve appears in an obvious stage III, indicating that the volume of the broken rock is larger when the cutting depth is deeper and has high rock breaking efficiency. As shown in Fig. 12(b), as the cutting angle increases, although the lengths of stages I and II increase slightly, it does not cause the reduction of stage III, on the contrary, it becomes longer with the cutting angle increases, indicating that the machete cutter affects a larger rock volume during the rock breaking process with the angle increases.

By comparing the cutting force versus displacement curves of the three types of cutters, the rock-breaking process of the cutter can be divided into the cutter pressing process (stage I), the cutter's rapid rock-breaking process (stage II), the cutter's stable rock-breaking process. (stage III) and the preparatory rock-breaking process of the cutter (stage IV). When the cutter have completely broken the rock, stage I and stage IV will overlap to form a stage, which represents the stage of pressing in new unbroken rock. Together with stage II, it constitutes the fluctuation stage in the PDC cutting process. Large pieces of cuttings are generated in stages I, II and IV. A large amount of energy is consumed and the cutting force is very large during the cutting process in these three stages, making the cutting process unstable. stage III is the stable cutting stage, where the cutting force required is very small and the rock is plastically broken. Therefore, the SI index of the PDC cutter can be obtained by analyzing the changes in the stable stage and Fluctuation stage, and the parameter optimization of the PDC cutter can be completed by combining the change rules of MSE.

Parameter optimization based on SI and MSE

As shown in Fig. 13, the average cutting force F_a of the stable stage, the maximum cutting force F_{max} of the Fluctuation stage, and the average cutting force F_{avg} of the two stages were compared for the three PDC cutters at different cutting depths. It can be seen from the cutting force change curve that the three cutting forces are relatively close when the cutting depth is low ($d < 1$ mm), indicating that the working state of the PDC cutter is relatively stable at this time. The reason is that due to the shallow cutting depth, most of the rock It is plastic failure, and it is difficult to generate large cuttings, and there is no brittle failure that requires sudden consumption of a large amount of cutting force. At this time, although the shapes of the PDC cutters are very different, the difference in cutting force is not significant, which shows that the range of the crushing zone of each cutter is similar under the condition of shallow cutting depth. When the cutting depth is deeper ($d > 2$ mm),

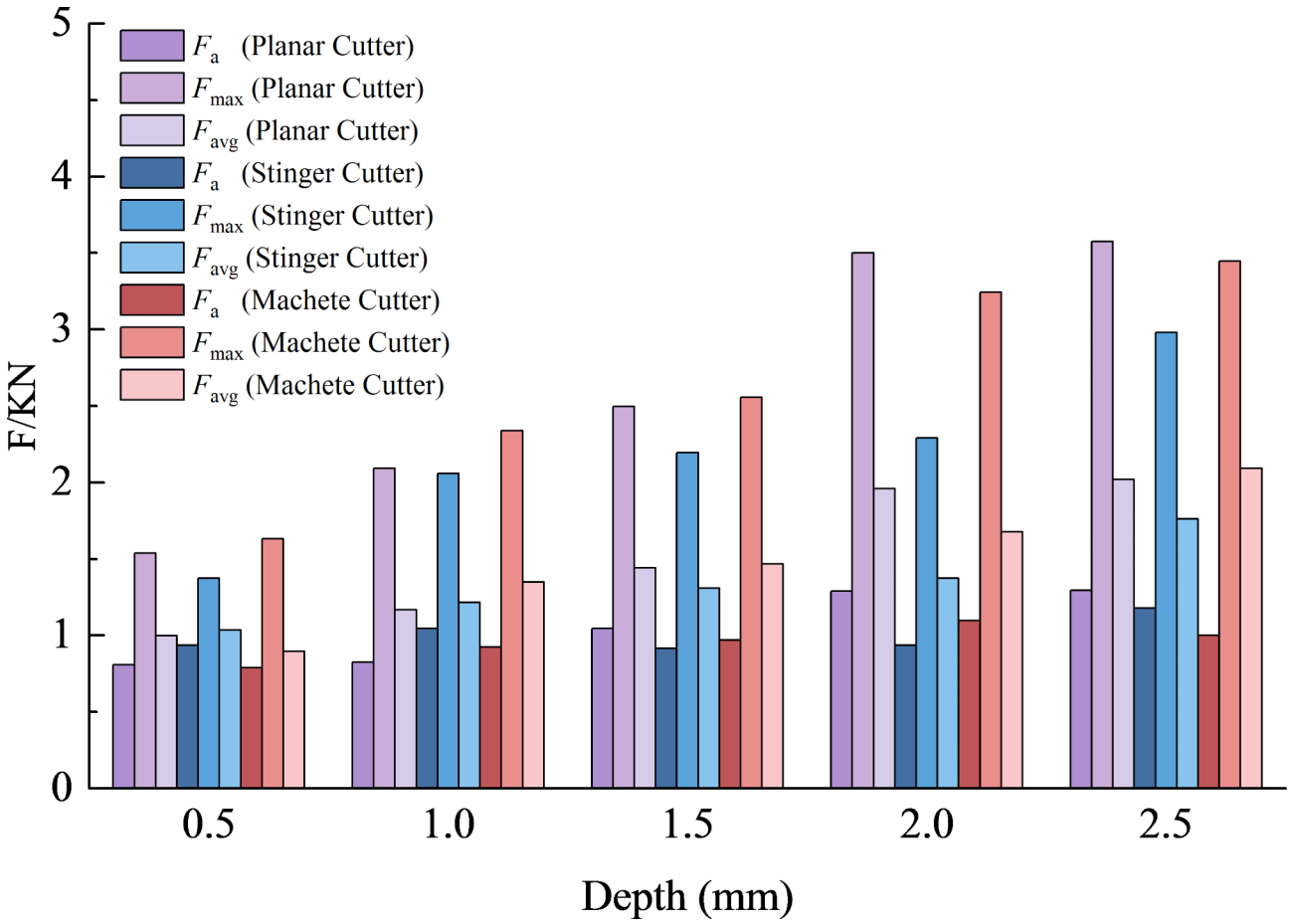

Fig. 13. Statistics on the changes of cutting force with cutting depth.

the cutting forces of the cutters fluctuate significantly. First, the F_{max} of the planar cutter and machete cutter increases sharply. This is because the rock-breaking area of the cutters increased significantly. The increase in the rock-breaking area will cause the cutters to break the rock with greater strength when peeling off the upper rock in the cutter tip crushing zone, so the cutting force required increases. At this time, the rock failure mode is plastic failure and brittle failure occurring simultaneously. It can be seen that as the cutting depth increases, F_{max} increases significantly faster than F_a, indicating that the cutters become more and more unstable as the cutting depth increases, so the cutting depth of the PDC cutters cannot be too large.

As shown in Fig. 14, it is the variation curve of MSE and SI with cutting depth. MSE represents the average energy consumed in breaking a unit volume of rock. The lower the MSE, the higher the rock breaking efficiency of the PDC cutter. It can be seen from the change pattern of MSE that the main influence on MSE is the rock breaking area of the cutter. At the same cutting depth, the rock breaking efficiency of the planar cutter is the highest, and the rock breaking efficiency of the stinger cutter is the lowest. This is also because the planar cutter have a larger rock-breaking area, as the cutting depth increases, the rock-breaking efficiency of the cutter increases to a certain extent, and the gap in rock-breaking efficiency between the cutter becomes smaller and smaller. This shows that from the perspective of rapid drilling, the deeper the cutting depth and the cutter with a larger rock breaking area, the higher the rock breaking efficiency. However, since deeper cutting depth will cause severe fluctuations in cutting force and affect the stability of the cutter, it is necessary to use the stability index (SI) to evaluate the working status of the cutter and optimize the optimal cutting depth. It can be seen from the change of SI with cutting depth that the stability of the planar cutter is relatively balanced at different depths. When the cutting depth is 1.5 mm, the stability is better than other cutting depths. The stinger cutter has high stability when the cutting depth is shallow, but when the cutting depth is greater than 1 mm, its stability drops sharply, but compared with the other two PDC cutter, the stinger cutter's stability relatively good. Combined with the changes in cutting force in Fig. 11, it can be determined that the optimal cutting depth of the stinger cutter is 2 mm. At this time, the fluctuation of cutting force is not obvious and it has high rock breaking efficiency. The stability of the machete cutter will decrease rapidly when the cutting depth is greater than 2 mm, so its cutting depth should be less than 2 mm. Since the cutting force of the machete cutter will increase rapidly after the cutting depth is greater than 1.5 mm, the optimal cutting depth of the machete cutter is 1.5 mm.

As shown in Fig. 15, when the cutting depth of three PDC cutter is 2 mm, the average cutting force F_a of the stable stage, the maximum cutting force F_{max} of the fluctuation stage and the average cutting force F_{avg} of the

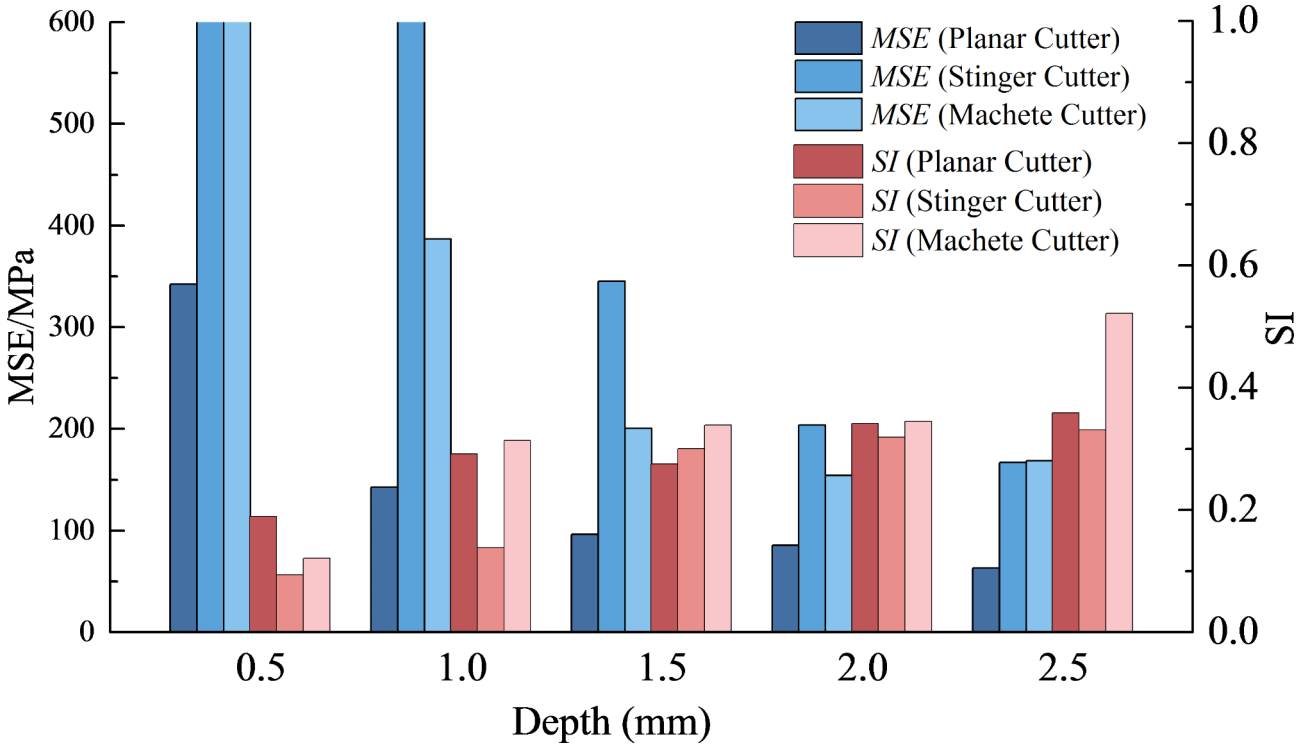

Fig. 14. Statistics on the changes of MSE and SI with cutting depth.

two stages under different cutting angles are compared. The influence of cutting angle on cutting force does not have a monotonically increasing law like cutting depth. The planar cutter has the highest sensitivity to the cutting angle. As the cutting angle increases, the cutting force gradually increases. When the cutting angle reaches 25°, an inflection point appears, and the cutting force rises rapidly and then drops rapidly. The F_{max} of the stinger cutter does not change significantly at each cutting angle, but its F_a and F_{avg} change in waves as the cutting angle increases. The cutting force of machete cutter increases rapidly when the cutting angle is less than 10°, and the cutting force remains stable when it is greater than 10°. The cutting angle only has a higher impact on the planar cutter.

As shown in Fig. 16, it is the variation curve of MSE and SI with cutting angle. The optimal cutting angle of the cuter is determined based on the changing rules of MSE and SI. The rock-breaking efficiency of the planar cutter does not change much with the cutting angle. However, when the cutting angle is greater than 20°, the stability of the cutter will become worse. Therefore, the cutting angle of the planar cutter is less than 20°.

The stinger cutter has the best stability when the cutting angle is 20°, which is the optimal cutting angle of the stinger cutter. At the same time, it can be seen that cutting angle will make the stability of the stinger cutter worse. This is because the rock breaking process of the stinger cutter is relatively special, and the rock is broken in a plowing manner, which causes the cutting force fluctuations to be very obvious when the back rake angle is small or large.

The SI value of the machete cutter shows a trend of first increasing and then decreasing as the cutting angle increases, reaching the maximum value at 15°. This may be related to the structure of the machete cutter. Their rock breaking is more dependent on stress concentration. Too large a rake angle will reduce the effect of stress concentration, thereby reducing the cutting force and making the cutter more stable. Combined with the changing law of cutting force in Fig. 14, the cutting force of the machete cutter The angle should be less than 10°.

Figures 14 and 16 indicate that at shallow cutting depths, the variation in cutting force is negligible, reflected by an SI value of 1, suggesting high stability of the cutter. As the cutting depth increases, the cutting force exhibits noticeable intermittent fluctuations, and the SI value progressively decreases, indicating a gradual reduction in the stability of the cutter.

The main function of the parameter SI is to monitor the stress state of the PDC cutter and then optimize the working parameters of the PDC cutter. When the plastic damage is mostly in the rock, the value of the parameter SI is very small and the cutting force that the PDC cutter need to provide is small. When the rock undergoes brittle failure, the cutting force will change in a fluctuating manner. At this time, the value of the parameter SI gradually increases. Since the cutter are continuously subjected to strong damage, they are more likely to be worn or even damaged. As the penetration depth of the PDC cutter increases, the MSE gradually decreases while the SI value continues to increase. This means that drilling efficiency and the stability of the PDC cutter are not compatible, but the optimal work can be determined by observing changes in SI. The parameters enable the PDC cutter to have strong stability while maintaining drilling efficiency.

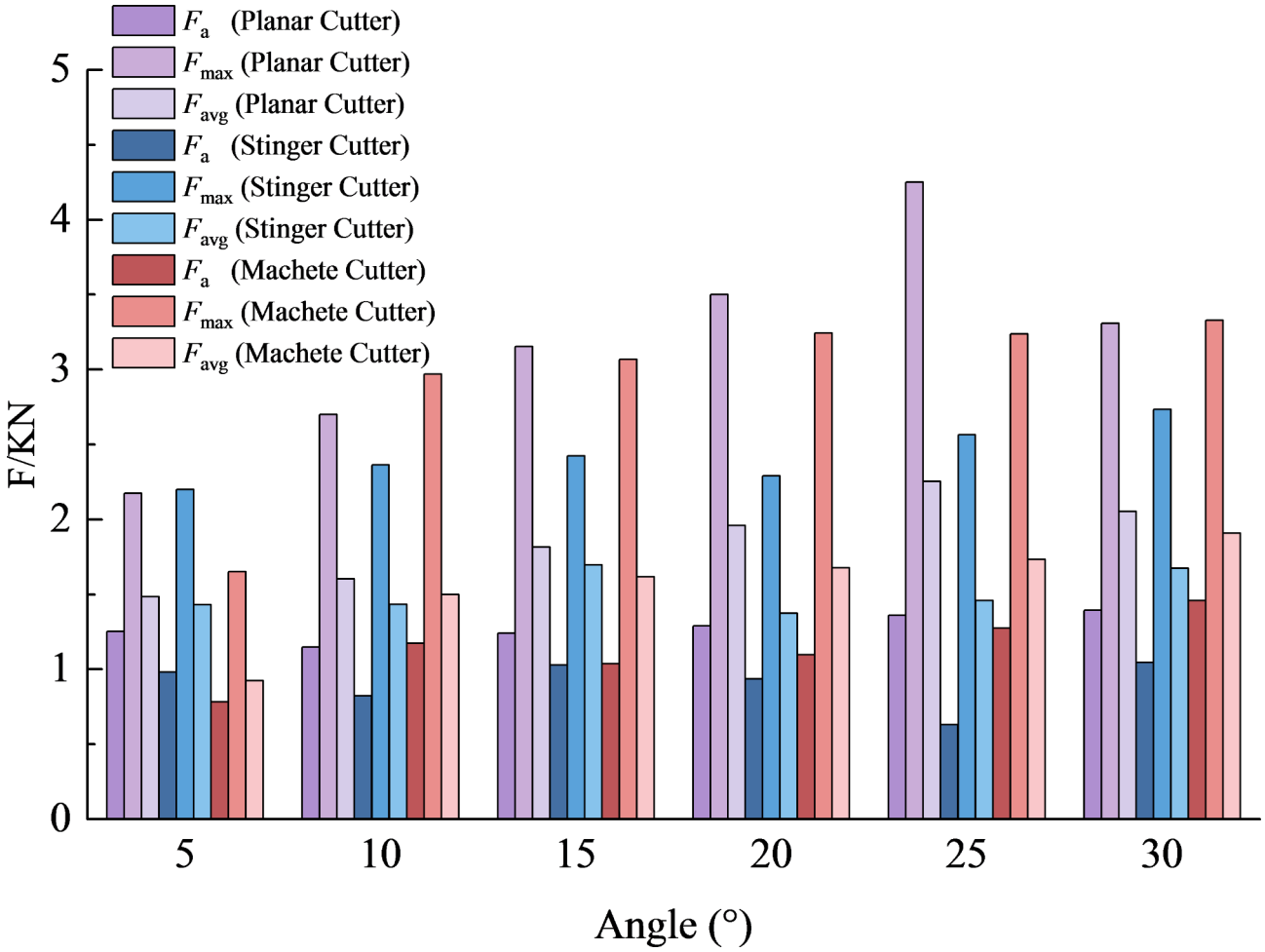

Fig. 15. Statistics on the changes of cutting force with cutting angle.

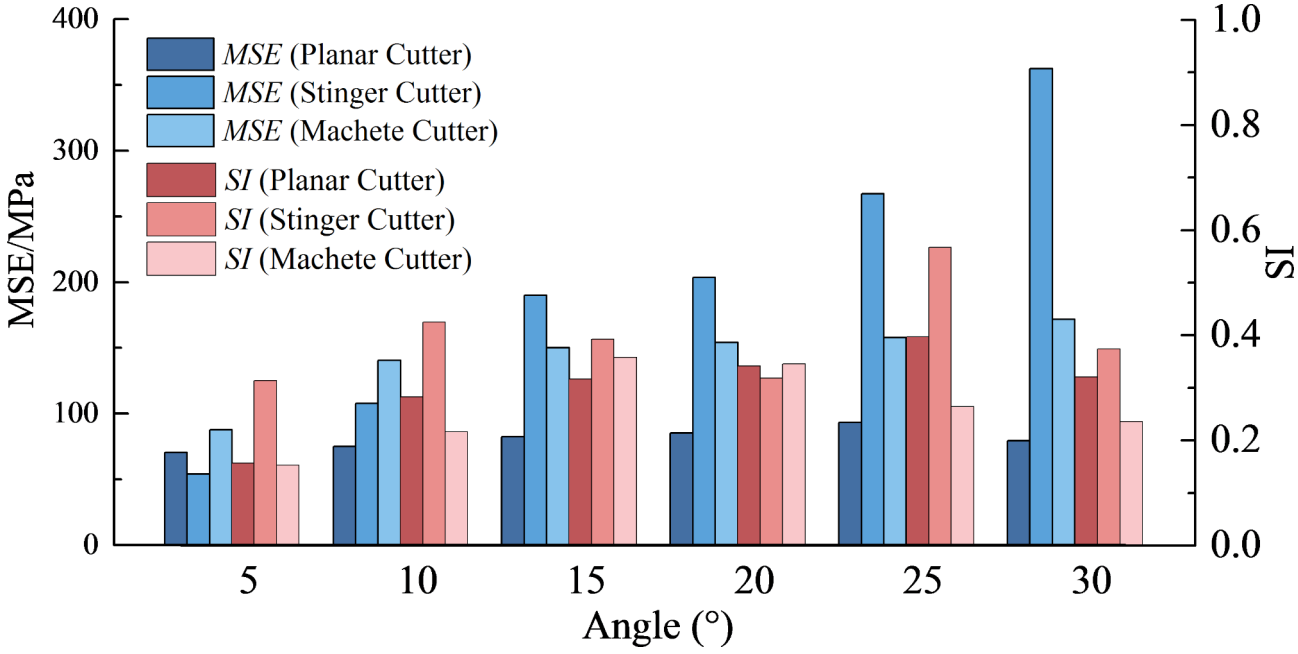

Fig. 16. Statistics on the changes of MSE and SI with cutting angle.

Conclusions

In this article, a rock-breaking mechanism model of PDC cutter is established based on the way in which PDC cutter breaking rock, and a cutter stability index SI is proposed. The FDEM method was used to simulate the rock breaking process of planar cutter, machete cutter and stinger cutter under different cutting depths and cutting angles, and the parameters SI and MSE were used to optimize the optimal working parameters of the three cutters. The main conclusions drawn are as follows.

[1] At shallow cutting depths, cutting force variations are minimal, and the Stability Index (SI) remains high, indicating stable cutter performance. As the cutting depth increases, cutting force fluctuations become pronounced, and the SI decreases, reflecting reduced cutter stability.

[2] The stability and efficiency of the cutters are influenced by cutting depth and angle. The optimal cutting depths are determined to be 2 mm for the stinger cutter and 1.5 mm for the machete cutter. The planar cutter maintains balanced stability across varying depths, with a slight preference for a depth of 1.5 mm. Optimal cutting angles are less than 20° for the planar cutter, 20° for the stinger cutter, and less than 10° for the machete cutter.

[3] The Stability Index (SI) and Mechanical Specific Energy (MSE) are crucial in optimizing cutter performance. A lower MSE indicates higher rock-breaking efficiency, while an increasing SI signifies greater cutting force fluctuations and potential for cutter wear. Balancing SI and MSE is essential to achieve optimal drilling efficiency and cutter stability.

Data availability

The datasets used and/or analysed during the current study available from the corresponding author on reasonable request.

Received: 1 March 2024; Accepted: 11 October 2024
Published online: 15 October 2024

References

1. Lu, J., Weerasooriya, U. P. & Pope, G. A. Investigation of gravity-stable surfactant floods. *Fuel*. **124**, 76–84 (2014).
2. Liu, Y., Li, J., Wang, Z., Wang, S. & Dong, Y. The role of surface and subsurface integration in the development of a high-pressure and low-production gas field. *Environ. Earth Sci.* **73** (10), 5891–5904 (2015).
3. Zhongwei, D., Xiaolong, P. & Fanhua, Z. Comparison analyses between the linear and non-linear pressure-decline methods in cyclic solvent injection (CSI) process for heavy oil recovery. *Fuel*. **224**, 442–450 (2018).
4. Zhong, H. et al. Role of Alkali Type in Chemical loss and ASP-Flooding enhanced Oil Recovery in Sandstone formations. *SPE Reservoir Eval. Eng.* **23** (2), 431–445 (2020).
5. Amoco, B. P. Statistical Review of World Energy 2020. (2020). https://file.51baogao.cn/20200623/41c6a78730a59aed65e22b24a198e5ab.pdf
6. Brett, J. F., Warren, T. M. & Behr, S. M. Bit Whirl-A New Theory of PDC bit failure. *Spe Drill. Completion*. **27** (1), 158–164 (2012).
7. Feenstra Status of polycrystalline-diamond-compact bits: Part 1 - Development. journal of petroleum technology 1988.
8. Doshvarpassand, S., Richard, T. & Mostofi, M. Effect of groove geometry and cutting edge in rock cutting. *J. Petrol. Sci. Eng.* **151**, 1–12 (2017).
9. Zhu, X. H., Luo, Y. X. & Liu, W. The rock breaking and ROP increase mechanisms for single-cutter torsional impact cutting using DEM. *Pet. Sci.* **16** (5), 1134–1147 (2019).
10. Zhang, Z. et al. 3D numerical simulation study of rock breaking of the wavy PDC cutter and field verification. *J. Petrol. Sci. Eng.* **203**, 108578 (2021).
11. Fu, X., Huang, Z., Shi, H., Song, H. & Wu, H. Comparison of fracture characteristics of different PDC cutters penetrating carbonate rock. *Geoenergy Sci. Eng.* 223. (2023).
12. Shao, F., Liu, W., Gao, D. & Ye, Y. Study on rock-breaking mechanism of axe-shaped PDC cutter. *J. Petrol. Sci. Eng.* 205. (2021).
13. Liu, W., Meng, X., Weng, X., Shen, X. & Zhu, X. Rock-breaking performance of specially-shaped PDC cutters from a new insight into the damage beneath cutting groove. *GEOENERGY Sci. Eng.* **231**, 212326 (2023).
14. Xiong, C. et al. 'Investigations on the Stinger PDC cutter breaking granitoid under in-situ stress and hydrostatic pressure conditions', *INTERNATIONAL JOURNAL OF ROCK MECHANICS AND MINING SCIENCES*, 164: 105312. (2023).
15. Xiong, C. et al. Performances of a Stinger PDC cutter breaking granite: cutting force and mechanical specific energy in single cutter tests. *Pet. Sci.* **20**, 1087–1103 (2023).
16. Zhu, X. et al. Rock cutting mechanism of special-shaped PDC cutter in heterogeneous granite formation. *J. Petrol. Sci. Eng.* **210**, 110020 (2022).
17. Bifano, T. G., Thomas, A., Dow & Ronald, O. S. 'Ductile-regime grinding: a new technology for machining brittle materials'. (1991).
18. Dai, X., Huang, Z., Shi, H. & Wu, X. and Chao Xiong. 'Cutting force as an index to identify the ductile-brittle failure modes in rock cutting', *INTERNATIONAL JOURNAL OF ROCK MECHANICS AND MINING SCIENCES*, 146: 104834. (2021).
19. Verhoef, P. N. W., Ockeloen, J. J. & Kesteren, W. G. M. V. The significance of rock ductility for mechanical rock cutting. *Rock. Mech. Tools Tech.* **1**, 709–716 (1996).
20. Zhou, Y. & Jeen-Shang, L. 'On the critical failure mode transition depth for rock cutting', *INTERNATIONAL JOURNAL OF ROCK MECHANICS AND MINING SCIENCES*, 62: 131 – 37. (2013).
21. Richard, T., Dagrain, F., Poyol, E. & Emmanuel Detournay. Rock strength determination from scratch tests. *Eng. Geol.* **147–148**, 91–100 (2012).
22. Chen, Z. et al. Hydraulic parameters optimization of two-stage PDC bit in deep formation applications. *GEOENERGY Sci. Eng.* **230**, 212248 (2023).
23. Bishop, R. F., Rodney Hill & Mott, N. F. 'The theory of indentation and hardness tests', *Proceedings of the Physical Society*, 57: 147. (1945).
24. Evans, I. The force required to cut coal with blunt wedges. *Int. J. Rock. Mech. Min. Sci. Geomech. Abstracts*. **2**, 1–12 (1965).
25. Hill, R., Lee, E. H. & Tupper, S. J. 'The theory of wedge indentation of ductile materials', *Proceedings of the Royal Society of London. Series A. Mathematical and Physical Sciences*, 188: 273 – 89. (1947).
26. Liu, W., Luo, Y., Zhu, X. & Yang, F. 'The ductile–brittle failure mode transition of hard brittle rock cutting—new insights from numerical simulation', *Geomechanics and Geophysics for Geo-Energy and Geo-Resources*, 8: 129. (2022).
27. Kou, S. Q., Liu, H. Y., Lindqvist, P. A. & Tang, C. A. 'Rock fragmentation mechanisms induced by a drill bit', *INTERNATIONAL JOURNAL OF ROCK MECHANICS AND MINING SCIENCES*, 41: 527 – 32. (2004).

28. Richard, T. et al. Rock strength determination from scratch tests[J]. *Eng. Geol.* 147–148. https://doi.org/10.1016/j.enggeo.2012.07.011 (2012).
29. Liu, W., Deng, H., Zhu, X. & Deng, K. 'The PDC cutter-rock interaction behavior in rock cutting: A review'. *GEOENERGY Sci. Eng.* , 229. (2023).
30. Larson, D. A., Roger, J., Morrell & Joel, F. M. *An Investigation of Crack Propagation with a Wedge Indenter to Improve rock Fragmentation Efficiency* (US Department of Interior, Bureau of Mines), 1987).
31. Teale, R. The concept of specific energy in rock drilling. *Int. J. Rock. Mech. Min. Sci. Geomech. Abstracts*. **2**, 57–73 (1965).
32. Zou, J. & Han, J. and Weihao Yang. 'Investigating the Influences of Indentation Hardness and Brittleness of Rock-Like Material on Its Mechanical Crushing Behaviors', *Mathematical Problems in Engineering*, 2020: 1–16. (2020).
33. Gong, Q. M. & Zhao, J. 'Influence of rock brittleness on TBM penetration rate in Singapore granite', *TUNNELLING AND UNDERGROUND SPACE TECHNOLOGY*, 22: 317 – 24. (2007).
34. Shao, F., Liu, W., Gao, D. & Yuchen Ye Study on rock-breaking mechanism of axe-shaped PDC cutter. *J. Petrol. Sci. Eng.* **205**, 108922 (2021).
35. Jiang, H. et al. Numerical investigation of rock breaking by a dish-shape cutter with advance slotting. *Eng. Fract. Mech.* **289**, 109393 (2023).

Author contributions

Conceptualization, X.R., Z.D. and H.Z.; methodology, X.R., Z.D.; validation, H.Z., J.L. and Q, C.; formal analysis, X.R,; investigation, B.Y.; resources, H.Z. and J.L; data curation, Z.D; writing—original draft preparation, X.R.; writing—review and editing, H.Z.; visualization, X.R, and Y.Z.; supervision, H.Z.; project administration, H.Z.; funding acquisition, H.Z. All authors reviewed the manuscript.

Funding

This research was supported by the National Natural Science Foundation of China (Grant No. 52174010, 52227804), Strategic Cooperation Technology Projects of CNPC and CUPB (Grant No. ZLZX2020-01), Sinopec key laboratory of drilling completion and fracturing of shale oil and gas (Grant No. 35800000-22-ZC0699-0004), Key Projects of Scientific Research Plan in Colleges and Universities of Xinjiang Uygur Autonomous Region (Grant No.XJEDU20211028).

Declarations

Competing interests

The authors declare no competing interests.

Additional information

Correspondence and requests for materials should be addressed to H.Z.

Reprints and permissions information is available at www.nature.com/reprints.

Publisher's note Springer Nature remains neutral with regard to jurisdictional claims in published maps and institutional affiliations.